

SDSS J1619 with blue-shifted broad components in H α and in [O III] having similar line width and velocity shifts: a recoiling SMBH candidate?

Xue-Guang Zhang^{*}

Guangxi Key Laboratory for Relativistic Astrophysics, School of Physical Science and Technology, Guangxi University, Nanning, 530004, P. R. China

1 February 2024

ABSTRACT

In this Letter, we report a potential candidate of recoiling supermassive black hole (rSMBH) in SDSS J1619 based on similar velocity shifts and line widths of the blue-shifted broad components in H α and [O III] doublet. The measured line width ratio between blue-shifted broad H α and broad [O III] line is 1.06, if compared with common values around 5.12 for normal Type-1 AGN, indicating different properties of the blue-shifted broad components in SDSS J1619 from those of normal QSOs. The virial BH mass M_{BHr} derived from the broad H α is consistent with the mass expected from the $M_{BH} - \sigma$ relation. The similar velocity shifts and line widths of the blue-shifted broad components in H α and [O III] and the virial BH mass derived from the H α broad line emissions that is consistent with the mass expected from the $M_{BH} - \sigma$ relation, can be explained by a rSMBH scenario. Besides the rSMBH scenario, either the similar line widths of the blue-shifted broad components in H α and in [O III] or the consistency between the virial BH mass and the mass expected from the $M_{BH} - \sigma$ relation cannot be explained by the other proposed models in SDSS J1619.

Key words: active galactic nuclei – emission line galaxies – supermassive black holes – quasars

1 INTRODUCTION

A black hole (BH) can be kicked away from central region of an active galactic nuclei (AGN), due to gravitational wave carrying away linear momentum, as discussed in Merritt et al. (2006); Volonteri (2007); Blecha & Loeb (2008); Komossa & Merritt (2008); Gualandris & Merritt (2008); Blecha et al. (2016); Zakaria et al. (2017); Shen et al. (2019). The BH being kicked away is also called as gravitational wave recoiling supermassive BH (=rSMBH), leading to the known off-nucleus AGN with shifted broad emission lines due to materials in broad emission line regions (BLRs) bound to the recoiling BH. Until now, tens of AGN have been reported with blue-shifted broad lines.

SDSS J0927+2943 at redshift 0.713 has been firstly reported in Komossa et al. (2008) with rSMBH expected blue-shifted velocity 2650km/s in low/high-ionization broad emission lines. However, a binary black hole (BBH) system can also lead to the blue-shifted lines in SDSS J0927+2943, as discussed in Bogdanovic et al. (2009). SDSS J1050 has been reported in Shields et al. (2009) with blue-shifted velocity 3500km/s in broad H β , however, BLRs lying into central accretion disk (disk emitter) would be preferred in SDSS J1050 to explain the shifted broad H β . Similar as the results in SDSS J0927+2943 and in SDSS J1050, there are blue-shifted broad lines reported in several individual AGN, such as SDSS J0956+5128 in Steinhardt et al. (2012), CXO J1015+6259 in Kim et al. (2017), SDSS J1056+5516 in Kalfountzou et al. (2017), Mrk1018 in Kim et al. (2018), 3C186 in Chiaberge et al. (2017, 2018), J0437+2456 in Pesce et al. (2021), etc., but the rSMBH scenario cannot be accepted as the unique scenario to explain the reported blue-shifted emission

lines. Meanwhile, besides reported individual AGN with blue-shifted broad emission lines, there are about 88 low redshift ($z < 0.7$) SDSS quasars reported with blue-shifted velocities larger than 1000km/s in broad H β in Eracleous et al. (2012); Runnoe et al. (2015, 2017), and rather than the rSMBH scenario, BBH systems would be preferred in fraction of the low redshift quasars. Therefore, not only rSMBH scenario, but also BBH system, disk emitter or probable outflowing model can be applied to explain shifted broad emission lines in AGN.

Currently, there are probably two main reasons which affect the plausibility of the rSMBH scenario. First, when a rSMBH is kicked away in AGN, probably not total materials in central BLRs are carried away with the rSMBH, but part of BLRs should be probably left in central region of AGN. In other words, there are two components in observed broad Balmer emission lines, one component from the BLRs bound to the rSMBH and the other component related to the materials in BLRs left in central region, leading to more complicated profiles of observed broad emission lines which not only include contributions from rSMBH expected blue-shifted broad components but also include rSMBH-independent components. How to effectively ignore effects of rSMBH-independent components is a challenge on studying properties of rSMBH expected blue-shifted broad emission features. However, considering the rSMBH-independent broad emission components coming from the left part of BLRs in central regions of AGN, it will be preferred to detect and study rSMBH-expected blue-shifted broad emission lines in Type-1.9 AGN, because rSMBH-independent broad emission components can be heavily obscured as many as possible by central dust torus. Second, as discussed in Merritt et al. (2006); Komossa & Merritt (2008); Gualandris & Merritt (2008); Blecha & Loeb (2011); Blecha et al. (2016), the rSMBH may be off-nucleus for 10^{6-9} years with 1pc-1kpc distance from the center. Meanwhile, as discussed in Liu et al. (2013a); Hainline et al.

^{*} Corresponding author Email: xgzhang@gxu.edu.cn

Table 1. Line parameters of each Gaussian emission component

line	λ_0	σ	flux
Broad H α	6549.52 \pm 5.61	19.76 \pm 3.35	284 \pm 68
Broad H β	4851.51 \pm 4.16	14.64 \pm 2.48	23 \pm 8
Narrow H α	6571.31 \pm 0.12 6559.15 \pm 0.28	4.85 \pm 0.16 2.29 \pm 0.31	537 \pm 45 51 \pm 10
Narrow H β	4867.64 \pm 0.09 4858.63 \pm 0.21	3.59 \pm 0.12 1.70 \pm 0.23	81 \pm 4 7 \pm 2
[O III] λ 5007 \AA	5012.63 \pm 0.15 5004.44 \pm 0.37 4991.86 \pm 0.79	3.89 \pm 0.31 3.25 \pm 0.24 14.22 \pm 0.56	121 \pm 15 100 \pm 13 272 \pm 12
[N II] λ 6583 \AA	6591.80 \pm 0.46 6587.23 \pm 3.28	4.55 \pm 0.62 8.18 \pm 1.65	223 \pm 100 208 \pm 96

Notice: The first column shows which line is measured. The Second, third, fourth columns show the measured line parameters: the center wavelength λ_0 in units of \AA , the line width (second moment) σ in units of \AA and the line flux in units of $10^{-17} \text{ erg/s/cm}^2$.

(2013); Fischer et al. (2018); Dempsey & Zakamska (2018); Zhang (2022a), narrow emission line regions (NLRs) of AGN extend up to 1 kpc (NLRs sizes) from the central BHs. Therefore, a rSMBH with bounded materials related to central BLRs can reach NLRs in AGN, leading part of emission materials in NLRs to co-move with the rSMBH, strongly indicating that narrow emission lines should have similar shifted velocities and similar line widths as those of rSMBH expected blue-shifted broad emission lines. Unfortunately, there are so far no reports on effects of rSMBH on properties of narrow emission lines from NLRs. Considering the two main reasons above, it is interesting to detect blue-shifted components both in BLRs and NLRs.

Therefore, in this Letter, a special Type-1.9 AGN, SDSS J161950.67+500535.31 (=SDSS J1619), is reported with similar line widths and similar velocity shifts of blue-shifted broad components in both [O III] doublet and H α , suggesting a rSMBH scenario in SDSS J1619. This Letter is organized as follows. Section 2 and 3 show the analysis of the spectrum and the necessary discussions. Section 4 shows our final conclusions. And in this Letter, the cosmological parameters of $H_0 = 70 \text{ km} \cdot \text{s}^{-1} \text{ Mpc}^{-1}$, $\Omega_\Lambda = 0.7$ and $\Omega_m = 0.3$ have been adopted.

2 SPECTROSCOPIC RESULTS OF SDSS J1619

Motivated by our previous measurements of opening angle of central dust tours in a Type-1.9 AGN with double-peaked broad H α in Zhang (2022c), on studying properties of Type-1.9 AGN is one of our ongoing projects. Among our sample of Type-1.9 AGN, SDSS J1619 is selected as the subject of this Letter, due to its apparent blue-shifted broad components in both Balmer emission lines and forbidden [O III] lines.

SDSS spectrum (plate-mjd-fiberid=2884-54526-0145) of SDSS J1619 at $z \sim 0.283$ is collected from SDSS DR16 (Ahumada et al. 2021) and shown in Fig. 1 with median signal-to-noise about 12. The redshift is determined by the SDSS pipeline¹. Due to apparent stellar absorption features, host galaxy contributions should be

firstly determined and subtracted, in order to measure properties of narrow/broad emission lines. Based on the 39 simple stellar population templates from Bruzual & Charlot (2003); Kauffmann et al. (2003), the SSP (simple Stellar Population) method discussed and accepted in Cid Fernandes et al. (2005); Cappellari (2017); Zhang (2021a,b, 2022a,b) is applied to determine the host galaxy contributions. Meanwhile, besides the stellar templates, a fourth order polynomial function is applied to describe intrinsic AGN continuum emissions. Left panels of Fig. 1 show the best descriptions to the SDSS spectrum (with emission lines being masked out) of SDSS J1619 and the corresponding line spectrum (the SDSS spectrum minus the best descriptions) through the Levenberg-Marquardt least-squares minimization technique (the known MPFIT package), with $\chi^2/dof \sim 1.5$ (summed squared residuals divided by degree of freedom). Right panels of Fig. 1 shows clear descriptions to the absorption features around 4000 \AA . The determined stellar velocity dispersion (the broadening velocity for the stellar templates) is about 165 \pm 29km/s. Meanwhile, accepted the SDSS pipeline determined redshift 0.283, an additional shifted velocity about 500 \pm 20km/s for the stellar templates is needed to describe the stellar absorption features.

After subtractions of the stellar lights and the continuum emissions, emission lines around H β (from 4750 to 5150 \AA in rest frame) and around H α (from 6400 to 6700 \AA in rest frame) can be measured, similar as what we have recently done in Zhang (2021a,b, 2022a,b,c). Two broad Gaussian functions are applied to describe broad component in H β (H α). Two Gaussian functions plus one another Gaussian function are applied to describe the core components (with probable double-peaked features) and the component related to blue-shifted wing in each narrow emission line, including [O III] λ 4959, 5007 \AA doublet, narrow H β , [N II] λ 6548, 6583 \AA doublet and narrow H α . When the model functions above are applied, the following restrictions are accepted. First, corresponding components of the [O III] doublet (the [N II] doublet, or the narrow Balmer lines) have the same redshift and the same line widths in velocity space. Second, corresponding components in the broad Balmer lines have the same redshift and the same line widths in velocity space. Third, flux ratio of the [O III] doublet (the [N II] doublet) is fixed to the theoretical value 3. Fourth, each Gaussian component has intensity not smaller than zero. Then, Fig. 2 shows the best descriptions to the emission lines of SDSS J1619, through the MPFIT package, with $\chi^2/dof \sim 1.6$. The measured line parameters are listed in Table 1.

Based on the best fitting results, two points can be found. First, the observed flux ratio (Balmer Decrement) of broad H α to broad H β is about 12.35 $^{+11.12}_{-5.38}$ in SDSS J1619, quite larger than common values around 3.1 as shown in Vanden Berk et al. (2001); Dong et al. (2008) in normal Type-1 AGN, indicating SDSS J1619 can be classified as a Type-1.9 AGN. Second, blue-shifted broad components can be found in H α and also in forbidden [O III] doublet. Moreover, due to double-peaked features in [O III] λ 5007 \AA , it is hard to calculate velocity shifts of the broad component in [O III] λ 5007 \AA relative to the narrow component in [O III] λ 5007 \AA . Therefore, accepted the theoretical vacuum wavelength 6564.61 \AA and 5008.24 \AA for H α and [O III] λ 5007 \AA , the blue-shifted broad component in H α has shifted velocity 690 \pm 240km/s (calculated by central wavelength difference between the theoretical vacuum value and the measured value in Table 1) and second moment 900 \pm 170km/s, which are not quite different from the shifted velocity 980 \pm 50km/s and second moment 850 \pm 34km/s of the blue-shifted broad component in [O III] doublet, after considering uncertainties of the values. And the uncertainties of the velocity shifts and the second moments are calculated by the measured uncertainties (listed in Table 1) of the central wavelengths

¹ <https://www.sdss3.org/dr8/algorithms/redshifts.php>

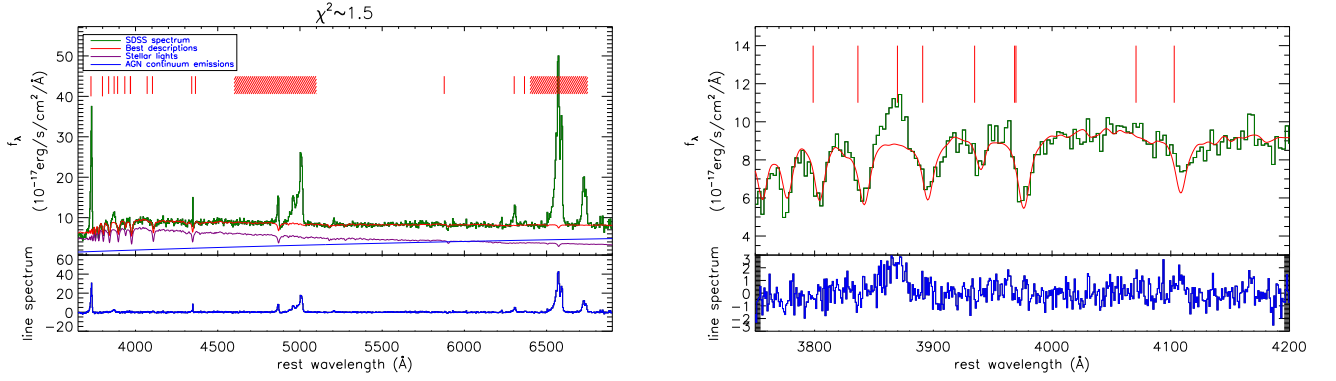


Figure 1. Left panel shows the SDSS spectrum (in dark green) of SDSS J1619 and the SSP method determined best descriptions (solid red line) to the spectrum with emission lines being masked out. In top region, as shown legend in top-left corner, solid purple line shows the SSP method determined stellar lights, solid blue line shows the continuum emissions, vertical red lines from left to right mark the following emission features masked out, including [O II] λ 3727Å, H θ , H η , [Ne III] λ 3869Å, He I λ 3891Å, Calcium K line, [Ne III] λ 3968Å, Calcium H line, [S II] λ 4070Å, H δ , H γ , [O III] λ 4364Å, He I λ 5877Å and [O I] λ 6300, 6363Å, respectively, and the area filled by red lines around 5000Å shows the region masked out including the emission features of probable He II, broad and narrow H β and [O III] doublet, and the area filled by red lines around 6550Å shows the region masked out including the emission features of broad and narrow H α , [N II] and [S II] doublets. Bottom region of left panel shows the line spectrum calculated by the SDSS spectrum minus sum of the stellar lights and the continuum emissions. Right panels show the best descriptions to the absorption features around 4000Å (rest wavelength range from 3750 to 4200Å) (top right panel) and the corresponding line spectrum (the SDSS spectrum minus sum of the stellar lights and the continuum emissions) (bottom right panel). In right panels, line styles and symbols have the same meanings as those in the left panels. In top right panel, vertical red lines from left to right mark the following emission features of H θ , H η , [Ne III] λ 3869Å, He I λ 3891Å, Calcium K line, [Ne III] λ 3968Å, Calcium H line, [S II] λ 4070Å, H δ .

and the second moments of the broad blue-shifted broad component in H α and in [O III] λ 5007Å.

Meanwhile, due to single-peaked feature in [N II] λ 6583Å, relative to the central wavelength of the core component in [N II] λ 6583Å, the shifted broad extended component with second moment about 370 ± 75 km/s and velocity shift about 208 ± 170 km/s can be found in [N II] doublet, quite smaller than the second moments and the velocity shifts of the blue-shifted broad components in H α and in [O III], indicating the blue-shifted components in [N II] doublet have quite different kinematic properties from those of the blue-shifted broad components in H α and in [O III]. Certainly, if accepted the theoretical vacuum wavelength 6585.27Å for [N II] λ 6583Å, the extended component in [N II] doublet should be red-shifted component, totally different properties from those of the blue-shifted broad components in H α and in [O III]. Therefore, the shifted broad components in [N II] doublet probably due to local kinematic properties of NLRs. There are no further discussions on the shifted components in [N II], besides the fitting results shown in Fig 2 and the line parameters listed in Table 1.

Furthermore, in Fig. 3, we show the distribution of the line width ratio R_{A3} between broad H α ($H\alpha_B$) and broad extended component (O3E) in [O III] line for the 535 normal QSOs (Zhang 2021a) with a mean value of $\log(R_{A3}) \sim 0.71 \pm 0.26$ (the standard deviation accepted as the uncertainty 0.26). The dashed vertical red line indicates the value for SDSS J1619 ($\sigma_{H\alpha_B}/\sigma_{O3E} = 900/850 \sim 1.06$). There is no QSO with R_{A3} smaller than the value for SDSS J1619, which implies that the probability of detecting QSOs with $R_{A3} < 1.06$ is lower than 1.87×10^{-3} (1/535) and suggests that SDSS J1619 is a unique source.

Finally, four velocity shifts measured for SDSS 1619 based on the SDSS redshift ($z = 0.283$) are listed in Table 2 with clear descriptions. And the velocity shifts SV of the broad components in H α and [O III] are mainly considered in the next section. If we adopt the stellar absorption feature as a reliable redshift of SDSS J1619 ($z = 0.285$),

the measured velocity shifts in Table 2 increase ($SV_{B,B} \sim 1080$ km/s and $SV_{B,O3} \sim 1370$ km/s) but the line widths do not change.

3 DISCUSSION

Based on the best fitting results, a blue-shifted broad component can be found in H α . However, it is necessary to determine where do the determined blue-shifted broad component in H α come from, from emission regions in NLRs or in BLRs.

Adopting the intrinsic flux ratio 3.1 of broad H α to broad H β , the observed flux ratio $12.35^{+11.12}_{-5.38}$ of broad H α to broad H β in SDSS J1619 indicates severe obscurations on the broad Balmer emission lines have $E(B - V) \sim 1.22^{+0.55}_{-0.49}$, leading the intrinsic broad blue-shifted component in H α to have line flux about $4405^{+1054}_{-3025} \times 10^{-17}$ erg/s/cm² (corresponding intrinsic line luminosity about $11.11^{+2.66}_{-7.61} \times 10^{42}$ erg/s). If accepted the blue-shifted broad component in H α tightly related to BLRs bound to the expected rSMBH in SDSS J1619, based on the virialization assumption (Vestergaard 2002; Peterson et al. 2004; Shen et al. 2011; Mejia-Restrepo et al. 2022), combining with the second moment 19.76 ± 3.35 Å of the blue-shifted broad H α and the improved empirical dependence (Bentz et al. 2013) of BLRs size on the intrinsic broad line luminosity (Greene & Ho 2005), virial mass of the recoiling BH in SDSS J1619 can be estimated by

$$M_{BHr} = 15.6 \times 10^6 \left(\frac{L_{H\alpha}}{10^{42} \text{ erg/s}} \right)^{0.55} \left(\frac{\sigma_{H\alpha}}{1000 \text{ km/s}} \right)^{2.06} M_{\odot} \\ = 4.75^{+2.64}_{-3.04} \times 10^7 M_{\odot} \quad (1)$$

with uncertainties determined by the uncertainties of line width and intrinsic line luminosity of the blue-shifted broad component in H α .

If the blue-shifted broad component in H α was not related to normal BLRs, the estimated M_{BHr} should be quite different from the BH mass expected from the $M_{BH} - \sigma$ relation in SDSS J1619. The $M_{BH} - \sigma$ relation discussed in Ferrarese & Merritt (2000);

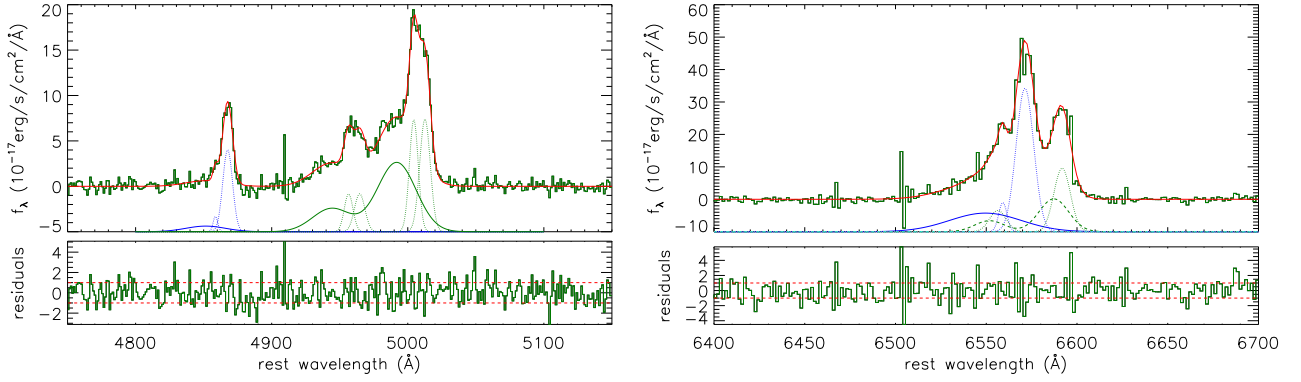


Figure 2. Top panels show the best fitting results (solid red line) to the emission lines in the line spectrum (solid dark green line), bottom panels show the corresponding residuals calculated by the line spectrum minus the best fitting results and then divided by uncertainties of the SDSS spectrum. In top left panel, dotted blue lines show the two components in narrow $H\beta$, dotted line in dark green and solid line in dark green show the double-peaked features and the blue-shifted broad component related to wings in $[O\ III]$ doublet, solid blue line shows the broad component in $H\beta$. In top right panel, dotted blue lines show the two components in narrow $H\alpha$, solid blue line shows the blue-shifted broad component in $H\alpha$, dotted lines in dark green and dashed lines in dark green show the core components and the blue-shifted component related to wings in $[N\ II]$ doublet. In each bottom panel, horizontal dashed lines show residuals= ± 1 , respectively.

Table 2. Shifted velocities SV listed in this Letter

value	description
$SV_{SSP} = 500 \pm 20\text{km/s}$	SSP method determined velocity shift for the Stellar Templates to describe absorption features in the SDSS spectrum with respect to $z \sim 0.283$
$SV_{B,B} = 690 \pm 240\text{km/s}$	Shifted velocity for the broad component in $H\alpha$, calculated by wavelength difference between the measured central wavelength of broad $H\alpha$ in rest frame ($z \sim 0.283$) and the theoretical vacuum wavelength 6564.61\AA
$SV_{B,O3} = 980 \pm 50\text{km/s}$	Shifted velocity for the broad component in $[O\ III]$, wavelength difference between the measured central wavelength of the broad component in $[O\ III]\lambda 5007\text{\AA}$ in rest frame ($z \sim 0.283$) and the theoretical vacuum wavelength 5008.24\AA
$SV_{N2} = 370 \pm 75\text{km/s}$	Shifted velocity for the extended component in $[N\ II]$, relative to the core component in $[N\ II]\lambda 6583\text{\AA}$

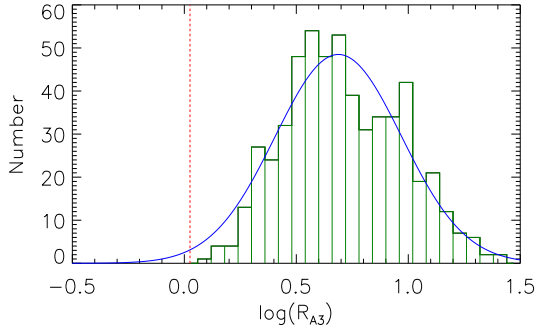


Figure 3. Distribution of line width ratio $\log(R_{A3})$ of broad $H\alpha$ to extended component in $[O\ III]\lambda 5007\text{\AA}$ of the 535 QSOs reported in Zhang (2021a). Vertical dashed red line shows $R_{A3} = 1.06$ for SDSS J1619. Solid blue line shows the Gaussian description to the distribution of $\log(R_{A3})$.

Gebhardt et al. (2000); Kormendy & Ho (2013); Batista et al. (2017); Bennert et al. (2021) can be conveniently applied to estimate central BH mass in both quiescent galaxies and active galaxies. Moreover, as discussed in Di Matteo et al. (2005); Johansson et al. (2009) for BBH systems at sub-pc scales, central total BH mass could be also estimated by the $M_{BH} - \sigma$ relation. Therefore, it is interesting

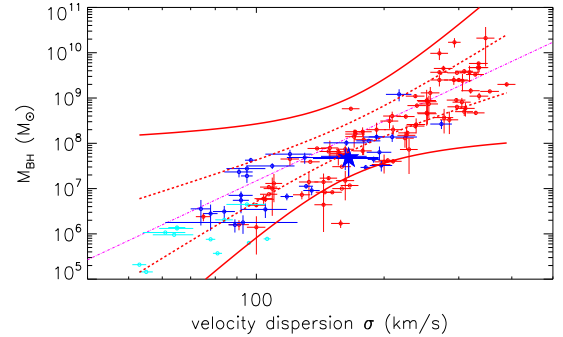


Figure 4. On dependence of BH mass on stellar velocity dispersion. Solid five-point-star with error bars in blue show the M_{BH} , and the velocity dispersion and corresponding uncertainties of SDSS J1619. Open circles in red, in blue and in cyan show the values for the 89 quiescent galaxies from Savorgnan & Graham (2015), the 29 RM AGNs from Woo et al. (2015) and the 12 TDEs from Zhou et al. (2021), respectively. Dot-dashed pink line, dashed red and solid red lines show the relation reported in Kormendy & Ho (2013) and the corresponding 3σ and 5σ confidence bands.

to check properties of the virial BH mass of SDSS J1619 in the plane of BH mass versus stellar velocity dispersion in Fig. 4. Here,

in order to show clearer results in Fig. 4, not only the $M_{\text{BH}} - \sigma$ relation reported in Kormendy & Ho (2013) is shown, but also the 89 quiescent galaxies from Savorgnan & Graham (2015) and the 29 reverberation mapped (RM) AGN from Woo et al. (2015) and the 12 tidal disruption events (TDEs) from Zhou et al. (2021) are also shown in the figure. Interestingly, in Fig. 4, $M_{\text{BH}r}$ of SDSS J1619 is consistent with the mass expected from the $M_{\text{BH}} - \sigma$ relation, based on the measured stellar velocity dispersion $165 \pm 29 \text{ km/s}$ in SDSS J1619. Therefore, the blue-shifted broad component in $\text{H}\alpha$ is from emission regions related to BLRs, and a rSMBH can be applied to explain the blue-shifted broad component in $\text{H}\alpha$.

Moreover, as discussed in Merritt et al. (2006); Gualandris & Merritt (2008); Komossa & Merritt (2008), materials can be bound to a rSMBH within a region with radius r_k given by

$$r_k \sim 512 \frac{M_{\text{BH}}}{10^8 M_{\odot}} \left(\frac{V_k}{10^3 \text{ km/s}} \right)^{-2} \text{light-days} \quad (2)$$

with M_{BH} and V_k as the BH mass and the kick velocity of a rSMBH. In SDSS J1619, based on the continuum luminosity at 5100\AA about $18.8^{+85.2}_{-14.7} \times 10^{44} \text{ erg/s}$ after considering the severe obscuration with $E(B-V) \sim 1.22^{+0.55}_{-0.49}$, the expected BLRs size is about $184^{+261}_{-108} \text{ light-days}$. Considering the $M_{\text{BH}r} \sim 4.75 \times 10^7 M_{\odot}$ in SDSS J1619, $V_k \sim 900 \text{ km/s}$ (the observed velocity shift) can lead to $r_k \sim 500 \text{ light-days}$, larger enough than the estimated BLRs size. In other words, the materials bound to the expected rSMBH in SDSS J1619 are enough to be applied to estimate the virial BH mass. Meanwhile, if accepted the new redshift 0.285 through the stellar absorption features, V_k should be corrected to $V_k \sim 1300 \text{ km/s}$, leading to $r_k \sim 250 \text{ light-days}$, still larger than the estimated BLRs size.

Therefore, considering the amplitude of parsecs to kilo-pcs of a rSMBH, when the rSMBH is wandering through the NLRs in SDSS J1619, the blue-shifted broad components in $[\text{O III}]$ doublet naturally have the same velocity shifts and the same line widths as those of the blue-shifted broad $\text{H}\alpha$ from the BLRs bound to the rSMBH. Before end of the section, besides the preferred rSMBH scenario in SDSS J1619, the other three probable models are simply discussed as follows.

First and foremost, there are double-peaked features in $[\text{O III}]\lambda 5007\text{\AA}$ doublet widely accepted as signs of dual core systems at kilo-pc scales (Zhou et al. 2004; Xu & Komossa 2009; Fu et al. 2011b; Wang et al. 2019). Based on the double-peaked features in $[\text{O III}]\lambda 5007\text{\AA}$, the peak separation is about $491 \pm 31 \text{ km/s}$, leading broad emission lines from central two cores to have the same peak separation $491 \pm 31 \text{ km/s}$. However, the velocity shift about 900 km/s of the blue-shifted broad $\text{H}\alpha$ in SDSS J1619 is about two times ($z \sim 0.283$ or $z \sim 0.285$ accepted) higher than the $491 \pm 31 \text{ km/s}$, indicating the blue-shifted broad $\text{H}\alpha$ is not related to a dual core system expected by the double-peaked $[\text{O III}]$ in SDSS J1619. Meanwhile, if a BBH system was assumed in SDSS J1619 without considerations of the double-peaked features in $[\text{O III}]\lambda 5007\text{\AA}$, a blue-shifted broad $\text{H}\alpha$ could be expected in SDSS J1619. However, it is hard to explain the blue-shifted broad components in $[\text{O III}]\lambda 5007\text{\AA}$ and in $\text{H}\alpha$ have the same line widths, as shown above that the probability is smaller than 1.87×10^{-3} to detect an AGN with $R_{\text{A3}} \leq 0.94$. Therefore, a BBH system is disfavoured in SDSS J1619.

Besides, a disk emitter (Chen & Halpern 1989; Eracleous et al. 1995; Storchi-Bergmann et al. 2003) can be applied to explain the blue-shifted broad $\text{H}\alpha$, however, it is also hard to explain the blue-shifted broad $\text{H}\alpha$ has the same line width as that of the blue-shifted broad component in $[\text{O III}]\lambda 5007\text{\AA}$ in SDSS J1619, due to lower probability 1.87×10^{-3} to find an AGN with $R_{\text{A3}} \leq 0.94$. Therefore, the BBH model is not favoured in SDSS J1619.

Last but not the least, an outflowing model could be applied to explain the similar velocity shifts and the similar line widths of the broad components in $\text{H}\alpha$ and $[\text{O III}]$ doublet, if accepted the broad components in $\text{H}\alpha$ and in $[\text{O III}]$ doublet were from NLRs. If the broad components were not from BLRs but from NLRs, it is hard to expect the consistency between the virial $M_{\text{BH}r}$ and the mass from the $M_{\text{BH}} - \sigma$ relation, while considering the probability lower around 1.87×10^{-3} to find an AGN with $R_{\text{A3}} \leq 0.94$. Therefore, the outflowing model is disfavoured in SDSS J1619.

4 CONCLUSIONS

After considering the advantages of studying rSMBH in Type-1.9 AGN, similar line widths and velocity shifts of the blue-shifted broad components in $\text{H}\alpha$ and $[\text{O III}]$ doublet are reported in the Type-1.9 AGN SDSS J1619. Based on the consistency between the central virial BH mass in SDSS J1619 and the BH mass expected from the $M_{\text{BH}} - \sigma$ relation, the blue-shifted broad $\text{H}\alpha$ can be accepted to come from BLRs bound to the expected rSMBH in SDSS J1619. Meanwhile, the expected rSMBH wandering through NLRs can be naturally applied to explain the similar velocity shifts and the similar line widths of the blue-shifted broad component in $\text{H}\alpha$ and in $[\text{O III}]$ in SDSS J1619. Therefore, the rSMBH scenario is preferred in SDSS J1619.

ACKNOWLEDGEMENTS

ZXG gratefully acknowledges the anonymous referee for reading our manuscript carefully and patiently, and giving us constructive comments and suggestions to greatly improve our paper. ZXG gratefully thanks the grant support from research funding by GuangXi University and the grant support from NSFC-12173020 and NSFC-12373014. The Letter has made use of the data from the SDSS projects with web site <http://www.sdss3.org/>. The Letter has made use of the MPFIT package (<http://cow.physics.wisc.edu/~craigm/idl/idl.html>) written by Craig B. Markwardt.

DATA AVAILABILITY

The data underlying this article will be shared on reasonable request to the corresponding author (xgzhang@gxu.edu.cn).

REFERENCES

- Ahumada, R.; Prieto, C. A.; Almeida, A.; et al., 2021, ApJS, 249, 3
 Batiste, M.; Bentz, M. C.; Raimundo, S. I.; Vestergaard, M.; Onken, C. A., 2017, ApJL, 838, 10
 Bennert, V. N.; Treu, T.; Ding, X.; et al., 2021, ApJ, 921, 36
 Bentz, M. C.; Denney, K. D.; Grier, C. J.; et al., 2013, ApJ, 767, 149
 Blecha, L.; Loeb, A. 2008, MNRAS, 390, 1311
 Blecha, L.; Cox, T. J.; Leob, A.; Hernquist, L., 2011, MNRAS, 412, 2154
 Blecha, L.; Sijacki, D.; Kelley, L. Z.; et al. 2016, MNRAS, 456, 961
 Bogdanovic, T.; Eracleous, M.; Sigurdsson, S., 2009, ApJ, 697, 288
 Bruzual, G.; Charlot, S. 2003, MNRAS, 344, 1000
 Cappellari, M.; Scott, N.; Alatalo, K., et al., 2013, MNRAS, 432, 1709
 Cappellari, M., 2017, MNRAS, 466, 798
 Chiaberge, M.; Ely, J. C.; Meyer, E. T.; et al., 2017, A&A, 600, 57
 Chiaberge, M.; Tremblay, G. R.; Capetti, A.; Norman, C., 2018, ApJ, 861, 56
 Chen, K. Y.; & Halpern, J. P., 1989, ApJ, 344, 115

- Cid Fernandes, R.; Mateus, A.; Sodre, L.; Stasinska, G.; Gomes, J. M., 2005, *MNRAS*, 358, 363
- Dempsey, R.; Zakamska, N. L., 2018, *MNRAS*, 477, 4615
- Di Matteo, T.; Springel, V.; Hernquist, L., *Natur*, 433, 604
- Dong, X.; Wang, T.; Wang, J.; Yuan, W.; Zhou, H.; Dai, H.; Zhang, K., 2008, *MNRAS*, 383, 581
- Eracleous, M., Livio, M., Halpern, J. P., Storchi-Bergmann, T., 1995, *ApJ*, 438, 610
- Eracleous, M.; Boroson, T. A.; Halpern, J. P.; Liu, J., 2012, *ApJS*, 201, 23
- Ferrarese, F.; Merritt, D., 2000, *ApJL*, 539, 9
- Fischer, T.; Kraemer, S.; Schmitt, H.; et al., 2018, *ApJ*, 856, 102
- Fu, H.; Zhang, Z.; Assef, R. J., et al., 2011b, *ApJL*, 740, 44
- Gebhardt, K.; Bender, R.; Bower, G., et al., 2000, *ApJL*, 539, 13
- Greene, J. E.; Ho, L. C., 2005, *ApJ*, 630, 122
- Gualandris, A.; Merritt, D., 2008, *ApJ*, 678, 180
- Hainline, K.; Hickox, R.; Greene, J.; et al., 2013, *ApJ*, 774, 145
- Johansson, P.; Naab, T.; Burkert, A., 2009, *ApJ*, 690, 802
- Kalfountzou, E.; Santos Lleo, M.; Trichas M., 2017, *ApJL*, 851, 15
- Kauffmann, G.; Heckman, T. M.; Tremonti, C., et al. 2003, *MNRAS*, 346, 1055
- Kim, D. C.; Yoon, I.; Privon, G. C.; Evans, A. S.; Harvey, D.; Stierwalt, S.; Kim, J. H., 2017, *ApJ*, 840, 71
- Kim, D. C.; Yoon, I.; Evans, A. S., 2018, *ApJ*, 861, 51
- Komossa, S.; Merritt, D., 2008, *ApJL*, 689, 89
- Komossa, S.; Zhou, H.; Lu, H., 2008, *ApJL*, 678, 81
- Kormendy, J.; Ho, L. C., 2013, *ARA&A*, 51, 511
- Liu G.; Zakamska, N.; Greene, J.; et al., 2013a, *MNRAS*, 430, 2327
- Mejia-Restrepo, J. E.; Trakhtenbrot, B.; Koss, M. J., et al., 2022, *ApJS*, 261, 5
- Merritt, D.; Storchi-Bergmann, T.; Robinson, A.; Batcheldor, D.; Axon, D.; Cid Fernandes, R., 2006, *MNRAS*, 367, 1746
- Peterson, B. M.; Ferrarese, L.; Gilbert, K. M., et al., 2004, *ApJ*, 613, 682
- Runnoe, J. C.; Eracleous, M.; Mathes, G.; et al., 2015, *ApJS*, 221, 7
- Runnoe, J. C.; Eracleous, M.; Pennell, A.; et al., 2017, *MNRAS*, 468, 1683
- Pesce, D. W.; Seth, A. C.; Greene, J. E.; et al., 2021, *ApJ*, 909, 141
- Savorgnan, G. A. D.; Graham, A. W., 2015, *MNRAS*, 446, 2330
- Shen, Y.; Richards, G. T.; Strauss, M. A.; et al., 2011, *ApJS*, 194, 45
- Shen, Y.; Hwang, H.; Zakamska, N.; Liu, X., 2019, *ApJL*, 885, 4
- Shields, G. A.; Rosario, D. J.; Smith, K. L.; et al., 2009, *ApJ*, 707, 936
- Steinhardt, C. L.; Schramm, M.; Silverman, J. D.; et al., 2012, *ApJ*, 759, 24
- Storchi-Bergmann, T.; Nemmen da Silva, R., Eracleous, M., et al., 2003, *ApJ*, 598, 956
- Vanden Berk, D. E.; Richards, G. T.; Bauer, A.; et al., 2001, *AJ*, 122, 549
- Vestergaard, M., 2002, *ApJ*, 571, 733
- Volonteri, M., 2007, *ApJL*, 663, 5
- Wang, M.; Luo, A.; Song, Y., et al., 2019, *MNRAS*, 482, 1889
- Woo, J.; Yoon, Y.; Park, S.; Park, D.; Kim, S. C., 2015, *ApJ*, 801, 38
- Xu, D.; Komossa, S., 2009, *ApJL*, 705, 20
- Zakaria M.; Yosuke M.; Hector O.; Oliver P.; Luciano R.; Ziri Y., 2017, *A&A*, 598, 38
- Zhang, X. G., 2021a, *ApJ*, 909, 16, ArXiv:2101.02465
- Zhang, X. G., 2021b, *ApJ*, 919, 13, ArXiv:2107.09214
- Zhang, X. G., 2022a, *ApJS*, 260, 31
- Zhang, X. G., 2022b, *ApJS*, 261, 23
- Zhang, X. G., 2022c, *ApJ*, 937, 105, ArXiv:2209.02164
- Zhang, X. G., 2022, *MNRAS*, 519, 4461, arXiv:2301.01957
- Zhou, H.; Wang, T.; Zhang, X.; Dong, X.; Li, C. 2004, *ApJL*, 604, L33
- Zhou, Z. Q.; Liu, F. K.; Komossa, S., et al., 2021, *ApJ*, 907, 77